

---

# Demographics-Informed Neural Network for Multi-Modal Spatiotemporal Forecasting of Urban Growth and Travel Patterns Using Satellite Imagery

---

Eugene K. O. Denteh<sup>1</sup>, Andrews Danyo<sup>1</sup>, Joshua Asamoah<sup>1</sup>, Blessing Agyei Kyem<sup>1</sup>, Armstrong Aboah<sup>1</sup>

<sup>1</sup>Department of Civil, Construction and Environmental Engineering,  
North Dakota State University, Fargo, ND 58102

eugene.denteh@ndsu.edu, andrews.danyo@ndsu.edu, joshua.asamoah@ndsu.edu,  
blessing.agyeikyem@ndsu.edu, armstrong.aboah@ndsu.edu

## Abstract

1 Spatiotemporal forecasting of urban growth requires models that explain not only  
2 where change occurs but why, linking built form to demographic dynamics and  
3 mobility outcomes. However, most models treat these signals in isolation, relying  
4 on static projections. To address this problem, we present a Demographics-  
5 Informed Neural Network (DINN) that integrates multiyear satellite imagery with  
6 demographic data for spatiotemporal prediction of urban growth. The study also  
7 leverages these learned demographic-spatial representations for travel behavior  
8 forecasting. DINN couples a DenseNet-style image predictor with gated residual  
9 connections and a demographic encoder fused at the bottleneck; a separately pre-  
10 trained demographic predictor serves as a frozen consistency regularizer during  
11 training, while its encoder transfers to a travel-behavior head predicting 16 mobility  
12 features. A multi-objective loss balances image fidelity, demographic consistency,  
13 and semantic consistency. Using satellite images from 2012-2023 paired with  
14 county-level American Community Survey data, DINN improves image quality  
15 (SSIM  $\approx 0.83$ ) and demographic coherence (Demo-loss  $\approx 0.14$ ), achieves strong  
16 demographic prediction (overall  $R^2 \approx 0.80$ ,  $>0.93$  for core population metrics),  
17 and delivers accurate travel behavior forecasts (overall  $R^2 \approx 0.91$ ). To validate the  
18 relevance of each architectural component in DINN, we conduct comprehensive  
19 ablation studies which effectively highlights the relevance of each model compo-  
20 nent. This study shows that the framework accurately forecasts spatiotemporal  
21 urban change and its associated demographics, linking where change occurs to its  
22 drivers and to resulting travel behavior.

## 23 1 Introduction

24 Spatiotemporal forecasting of urban growth requires an understanding of the fundamental relation-  
25 ships that exist between built environments, demographic characteristics, and travel behavior patterns  
26 [1–3]. These three components are fundamentally interconnected, as population dynamics drive  
27 land-use change, infrastructure development shapes residential patterns, and transportation networks  
28 structure mobility behaviors; yet conventional urban spatiotemporal analysis methods often treat  
29 them as isolated variables[4–6]. This fragmented approach has contributed to costly planning fail-  
30 ures, exemplified by projects such as the construction of Interstate 95 through Miami’s Overtown  
31 neighborhood, which displaced 10,000-12,000 residents and destroyed 40 blocks of established  
32 community infrastructure, resulting in substantial social disruption and economic losses[7]. Cur-

33 rent urban growth models predominantly rely on static projections that fail to capture the dynamic  
34 temporal relationships between demographic shifts, spatial transformations, and transportation pat-  
35 terns, limiting their effectiveness for sustainable development planning [8–10]. To address these  
36 limitations, this study introduces the Demographics-Informed Neural Network (DINN), a novel deep  
37 learning framework that integrates satellite imagery sequences with demographic data through an  
38 encoder-decoder architecture forecast future urban settings. DINN employs temporal gated residual  
39 connections to capture spatiotemporal dynamics, incorporates a frozen demographic predictor to  
40 enforce spatial-demographic consistency, and demonstrates transferability of learned representations  
41 through a travel behavior prediction network that utilizes frozen encoder weights.

## 42 2 Literature Review

43 Spatiotemporal urban growth studies range from cellular-automata models that simulate diffusion  
44 of land use [11–13] to deep spatiotemporal predictors that learn from image sequences using  
45 CNN-LSTM/ConvLSTM variants atop encoder-decoder backbones such as U-Net [14–16], yet  
46 most approaches append demographics rather than embed them in the representation, weakening  
47 cross-modal coherence. Building on evidence that built form strongly conditions travel demand and  
48 mode choice [17], recent mode-choice studies show that statistical and neural models with post-hoc  
49 explanation such as SHAP [18] outperform classical logit baselines [19, 20], yet they typically rely  
50 on tabular demographics and network summaries rather than spatial data, leaving the connection to  
51 imagery-derived representations underused. Moreover, recent multimodal fusion studies in remote  
52 sensing identify attention-based architectures as effective for combining heterogeneous inputs, while  
53 also noting persistent challenges in aligning modalities and enforcing cross-modal consistency [21].  
54 Complementing this, studies that fuse sociodemographic attributes with satellite imagery via deep hy-  
55 brid models show consistent gains when numeric and image features are embedded in a shared latent  
56 space, reinforcing the case for representation-level integration [22]. Therefore these studies highlight  
57 the need for a framework that (i) fuses imagery and demographics within the encoder-decoder,  
58 (ii) regularizes forecasts with demographic consistency, and (iii) transfers the learned demographic  
59 representation to travel-behavior prediction.

## 60 3 Problem Formulation

61 Despite the significant advancements in data-driven transportation planning methodologies, effectively  
62 modeling the dynamic and temporal relationship between geographic changes in satellite imagery  
63 and socio-demographic patterns remains a persistent challenge. This paper proposes the utilization of  
64 satellite image sequences and corresponding demographics to predict future spatial representations  
65 and also predict the future demographics and travel behavior. To effectively model the relationship  
66 between geographic changes in satellite images and demographic factors, we formalize the problem  
67 as follows. Specifically, let  $\{x_{t-n}, \dots, x_t\}$  denote a temporal sequence of  $(n+1)$  historical satellite  
68 images, where each image  $x_i \in \mathbb{R}^{H \times W \times C}$  comprises RGB channels,  $C$  with spatial dimensions  
69  $H \times W$  (height and width, respectively). Correspondingly, let  $\{d_{t-n}, \dots, d_t\}$  represent the associated  
70 demographic feature vectors, each  $d_i \in \mathbb{R}^f$  containing  $f$  socio-demographic variables. The objective  
71 is to predict the future satellite image  $\hat{x}_{t+1} \in \mathbb{R}^{H \times W \times C}$  and the future demographic vector  $\hat{d}_{t+1} \in$   
72  $\mathbb{R}^f$  by using the temporal sequence of past satellite images,  $\{x_{t-n}, \dots, x_t\}$  together with their  
73 corresponding demographics,  $\{d_{t-n}, \dots, d_t\}$  as input into a network that predicts the future year.  
74 The general methodology adopted to achieve the objective is described in section 4. This study also  
75 leverages the strong relationship that exists between demographics and travel behavior [22, 23] to  
76 develop a travel behavior prediction network that leverages transfer learning by using a pretrained  
77 demographic feature encoder along with a specialized decoder to predict travel behavior.

## 78 4 Method

79 **Demographics-Informed Neural Network (DINN):** As displayed in Figure 1, DINN integrates  
80 satellite image sequences  $\{x_{t-n}, \dots, x_t\}$  (each image  $x_i \in \mathbb{R}^{H \times W \times C}$ ) and the corresponding  
81 demographic feature vectors  $\{d_{t-n}, \dots, d_t\}$  (each vector  $d_i \in \mathbb{R}^f$ ) through a DenseNet-based  
82 encoder-decoder with gated residual connections. The encoder extracts hierarchical spatial features  
83  $E = \{E_1, \dots, E_7\}$ , while the demographic sequence is embedded as  $e_d \in \mathbb{R}^{512}$  and fused at

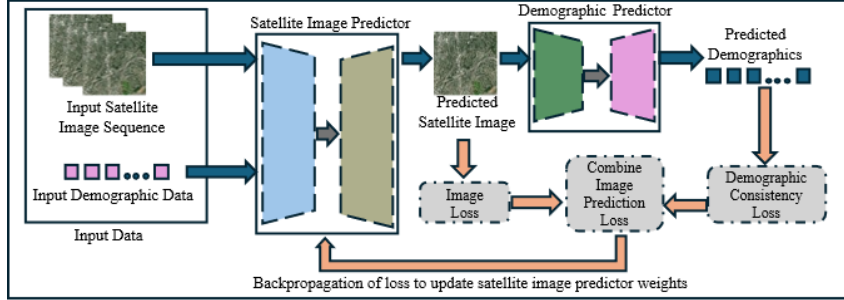


Figure 1: Demographics-Informed Neural Network (DINN)

84 the bottleneck as  $E_{\text{fused}} = \text{Conv}_{1 \times 1}([E_{\text{bottleneck}}, E_d])$ , where  $E_{\text{bottleneck}} \in \mathbb{R}^{H' \times W' \times C_b}$  and  
 85  $E_d = \text{tile}(e_d; H', W') \in \mathbb{R}^{H' \times W' \times 512}$  is the spatial broadcast of  $e_d$  across the bottleneck height  
 86 and width  $(H', W')$ . During decoding, gated residual connections  $G_i = \sigma(f_\theta([E_i, \text{Up}(D_{i+1})]))$   
 87 regulate feature flow between encoder and decoder, where  $\sigma(\cdot)$  denotes the sigmoid function,  $f_\theta$   
 88 is a  $1 \times 1$  convolution with batch normalization, and  $\text{Up}(\cdot)$  represents bilinear upsampling. The  
 89 predictor outputs the future satellite image  $\hat{x}_{t+1}$ , which is passed into a frozen demographic predictor  
 90 pre-trained to map imagery into demographics, producing  $\hat{d}_{t+1}$ . Training minimizes the combined  
 91 loss  $\mathcal{L} = \alpha \mathcal{L}_{\text{image}}(\hat{x}_{t+1}, x_{t+1}) + \beta \mathcal{L}_{\text{demo}}(\hat{d}_{t+1}, d_{t+1})$ , where  $\mathcal{L}_{\text{image}}$  blends perceptual and SSIM  
 92 terms for visual fidelity,  $\mathcal{L}_{\text{demo}}$  is a scale-normalized mean squared error enforcing demographic  
 93 alignment, and  $\alpha, \beta$  weight their contributions. This design ensures that spatial predictions are both  
 94 visually realistic and demographically consistent, with the frozen demographic predictor acting as the  
 95 key innovation that constrains the model to cross-modal coherence.

96 **Travel Behavior Prediction Network:** The travel behavior prediction network builds on the  
 97 demographic predictor by adopting its pre-trained encoder as a frozen feature extractor, thereby  
 98 preserving robust spatial–demographic mappings while avoiding overfitting. Specifically, the frozen  
 99 encoder  $f_{\text{frozen}} : \mathbb{R}^{H \times W \times C} \rightarrow \mathbb{R}^{h' \times w' \times c'}$  provides fixed bottleneck features that encode both spatial  
 100 context and demographic structure, ensuring that the downstream model inherits representations  
 101 already aligned with population characteristics. A trainable decoder reconstructs transportation-  
 102 specific patterns through transposed convolutions, while a global context pathway aggregates region-  
 103 wide signals using fully connected layers to capture broader mobility trends. The outputs are  
 104 concatenated and passed through a predictor head to produce the travel behavior vector  $\hat{t}_{t+1} \in \mathbb{R}^m$ ,  
 105 which includes attributes such as mode choice, vehicle availability, and travel times. Training  
 106 minimizes the objective  $\mathcal{L} = \mathcal{L}_{\text{travel}}(\hat{t}_{t+1}, t_{t+1}) + \gamma \mathcal{L}_{\text{semantic}}$ , where  $\mathcal{L}_{\text{travel}}$  is a scale-normalized mean  
 107 squared error across all  $m$  travel variables and  $\mathcal{L}_{\text{semantic}}$  preserves alignment between the decoder’s  
 108 embedding and the frozen encoder bottleneck. The key innovation lies in freezing the demographic  
 109 encoder which constrains the model to reuse learned demographic representations, the network  
 110 ensures that travel behavior forecasts remain demographically grounded while leveraging transfer  
 111 learning to improve generalization.

## 112 5 Experiments and Evaluation Metrics

113 We evaluate DINN on a multimodal dataset (2012–2023) comprising satellite imagery, demographics,  
 114 and travel behavior data for U.S. counties. Training used Adam ( $\text{lr} = 3 \times 10^{-4}$ , batch size 8) for  
 115 200 epochs on NVIDIA A100 GPU. Performance metrics include MSE for demographic/travel  
 116 predictions, SSIM/PSNR for image fidelity, and  $R^2$  for predictive accuracy. We also conduct ablation  
 117 studies and change heatmap evaluation to assess temporal robustness and spatial consistency.

## 118 6 Results and Discussion

119 **Demographic and Travel Behavior Predictor Performance:** As shown in Figure 2, the demo-  
 120 graphic predictor demonstrates strong performance across most population categories, achieving  $R^2$   
 121 values exceeding 0.90 for total and gender-specific populations, though comparatively lower accuracy

122 is observed for income- and inequality-related variables. This robust performance enables the demo-  
 123 graphic predictor to successfully enforce spatial-demographic consistency during training. Similarly,  
 124 the travel behavior predictor achieves high predictive accuracy across most mobility attributes, with  
 125 mode choice and vehicle availability well captured ( $R^2 > 0.95$ ) but walking remaining the most chal-  
 126 lenging attribute due to higher variance in spatial distribution. These results demonstrate successful  
 127 representation transfer from the frozen demographic encoder to behavioral forecasting, validating the  
 128 framework’s ability to leverage learned spatial-demographic relationships for cross-modal prediction  
 129 tasks.

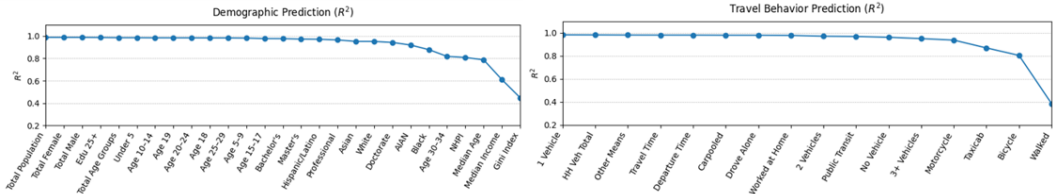


Figure 2: Line plots summarizing demographic predictor (Left) and Travel behavior Predictor (Right) test performance by feature.

130 **Ablation Study Results:** As illustrated in Figure 3, removing DenseNet blocks or gated skip  
 131 connections increases missed-change regions and spurious artifacts in the predictions (revealed  
 132 through the change heatmaps), while dropping the demographic predictor further disrupts demo-  
 133 graphic coherence. The quantitative trends in Table 1 mirror these effects with lower SSIM/PSNR  
 134 and higher Demo-Loss for ablated variants, whereas the full DInN attains the best scores across all  
 135 metrics, confirming each component’s contribution. Beyond architectural validation, the framework  
 136 successfully predicts subtle urban spatiotemporal changes that are typically difficult to identify  
 137 through visual inspection alone, leveraging change heatmaps that compute pixel-level differences  
 138 between temporal image sequences to quantify transformation patterns.

Table 1: Ablation study Results

Model Variant	Encoder Type	Gated Skip	Demographic Predictor	SSIM	PSNR (dB)	Demo-Loss
Baseline	2DConv	✗	✗	0.73	25.40	0.95
DInN-V1	2DConv	✓	✓	0.75	25.60	0.62
DInN-V2	Dense	✗	✓	0.78	25.77	0.33
DInN-V3	Dense	✓	✗	0.81	25.63	0.58
DInN	Dense	✓	✓	<b>0.83</b>	25.17	<b>0.14</b>

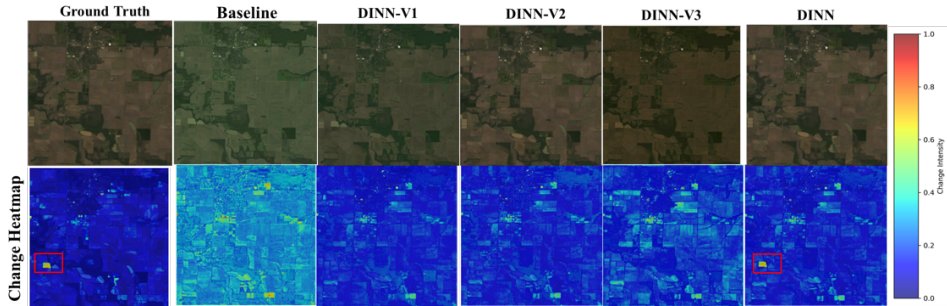


Figure 3: Qualitative ablation: top:inputs/predictions; bottom:change heatmaps. Red boxes highlight regions where ablations miss subtle changes; DInN preserves them.

## 139 7 Conclusion

140 This study demonstrates that integrating demographic context into spatiotemporal urban prediction  
 141 significantly enhances prediction accuracy, with the proposed DInN framework achieving remark-

142 able performance and validating co-evolutionary theories linking built environments and population  
143 characteristics. The strong predictive accuracy across demographic and travel behavior patterns  
144 confirms that spatial configurations encode sufficient information to forecast urban dynamics, providing  
145 planners with a practical tool that explicitly models demographic-spatial relationships for more  
146 equitable development strategies. The framework's ability to predict both where urban change occurs  
147 and it's corresponding demographics (why it occurs) represents a significant advancement toward  
148 evidence-based planning that can mitigate costly retrofitting and infrastructure obsolescence. Future  
149 research should extend validation beyond US metropolitan areas to diverse international contexts  
150 where demographic-spatial correlations may differ substantially.

## 151 **References**

152 [1] Reid Ewing and Robert Cervero. Travel and the built environment. *Journal of the American*  
153 *Planning Association*, 76(3):265–294, 2010. doi: 10.1080/01944361003766766. URL <https://doi.org/10.1080/01944361003766766>.

155 [2] Michael Wegener. Overview of land use transport models. In *Handbook of transport geography*  
156 and spatial systems, pages 127–146. Emerald Group Publishing Limited, 2004.

157 [3] Michael J Clay. Developing an integrated land-use/transportation model for small to medium-  
158 sized cities: case study of montgomery, alabama. *Transportation planning and technology*, 33  
159 (8):679–693, 2010.

160 [4] Robert Cervero and Kara Kockelman. Travel demand and the 3ds: Density, diversity, and  
161 design. *Transportation Research Part D: Transport and Environment*, 2(3):199–219, 1997.  
162 ISSN 1361-9209. doi: [https://doi.org/10.1016/S1361-9209\(97\)00009-6](https://doi.org/10.1016/S1361-9209(97)00009-6). URL <https://www.sciencedirect.com/science/article/pii/S1361920997000096>.

164 [5] John Bates and Jan Oosterhaven. Review of land-use/transport interaction models. *Department*  
165 *of the Environment, transport and the Regions*, 1999.

166 [6] Ransford A Acheampong and Elisabete A Silva. Land use–transport interaction modeling: A  
167 review of the literature and future research directions. *Journal of Transport and Land use*, 8(3):  
168 11–38, 2015.

169 [7] Raymond A Mohl. Interstating miami: Urban expressways and the changing american city.”.  
170 *Tequesta*, 68:193–226, 2008.

171 [8] Maher Milad Aburas, Yuek Ming Ho, Mohammad Firuz Ramli, and Zulfa Hanan Ash'aari.  
172 The simulation and prediction of spatio-temporal urban growth trends using cellular automata  
173 models: A review. *International Journal of Applied Earth Observation and Geoinformation*,  
174 52:380–389, 2016. ISSN 1569-8432. doi: <https://doi.org/10.1016/j.jag.2016.07.007>. URL <https://www.sciencedirect.com/science/article/pii/S0303243416301143>.

176 [9] Muhammad Asif, Jamil Hasan Kazmi, Aqil Tariq, Na Zhao, Rufat Guluzade, Walid Soufan,  
177 Khalid F. Almutairi, Ayman El Sabagh, and Muhammad Aslam. Modelling of land use and  
178 land cover changes and prediction using ca-markov and random forest. *Geocarto International*,  
179 38(1):2210532, 2023. doi: 10.1080/10106049.2023.2210532. URL <https://doi.org/10.1080/10106049.2023.2210532>.

181 [10] J. Ronald Eastman and Jiena He. A regression-based procedure for markov transition probability  
182 estimation in land change modeling. *Land*, 9(11), 2020. ISSN 2073-445X. doi: 10.3390/  
183 land9110407. URL <https://www.mdpi.com/2073-445X/9/11/407>.

184 [11] Michael G McNally. The four-step model. In *Handbook of transport modelling*, volume 1,  
185 pages 35–53. Emerald Group Publishing Limited, 2007.

186 [12] Agung Wahyudi and Yan Liu. Cellular automata for urban growth modelling: A review on  
187 factors defining transition rules. *International Review for Spatial Planning and Sustainable*  
188 *Development*, 4(2):60–75, 2016.

189 [13] Anthony GO Yeh, Xia Li, and Chang Xia. Cellular automata modeling for urban and regional  
190 planning. In *Urban informatics*, pages 865–883. Springer, 2021.

191 [14] Wadii Boulila, Hamza Ghadorh, Mehshan Ahmed Khan, Fawad Ahmed, and Jawad Ahmad.  
192 A novel cnn-lstm-based approach to predict urban expansion. *Ecological Informatics*, 64:  
193 101325, 2021. ISSN 1574-9541. doi: <https://doi.org/10.1016/j.ecoinf.2021.101325>. URL <https://www.sciencedirect.com/science/article/pii/S1574954121001163>.

195 [15] Jeong-Min Kim, JS Park, CY Lee, and SG Lee. Predicting of urban expansion using convolutional lstm network model: the case of seoul metropolitan area, korea. *ISPRS Annals of the Photogrammetry, Remote Sensing and Spatial Information Sciences*, 10:113–118, 2022.

196 [16] Olaf Ronneberger, Philipp Fischer, and Thomas Brox. U-net: Convolutional networks for  
197 biomedical image segmentation. In *International Conference on Medical image computing and  
200 computer-assisted intervention*, pages 234–241. Springer, 2015.

201 [17] Robert Cervero and Kara Kockelman. Travel demand and the 3ds: Density, diversity, and design.  
202 *Transportation research part D: Transport and environment*, 2(3):199–219, 1997.

203 [18] Scott M Lundberg and Su-In Lee. A unified approach to interpreting model predictions.  
204 *Advances in neural information processing systems*, 30, 2017.

205 [19] Li Tang, Chuanli Tang, Qi Fu, and Changxi Ma. Predicting travel mode choice with a robust  
206 neural network and shapley additive explanations analysis. *IET Intelligent Transport Systems*,  
207 18(7):1339–1354, 2024.

208 [20] Victoria Dahmen, Simone Weikl, and Klaus Bogenberger. Interpretable machine learning for  
209 mode choice modeling on tracking-based revealed preference data. *Transportation Research Record*,  
210 2678(11):2075–2091, 2024.

211 [21] Jiaxin Li, Danfeng Hong, Lianru Gao, Jing Yao, Ke Zheng, Bing Zhang, and Jocelyn Chanussot.  
212 Deep learning in multimodal remote sensing data fusion: A comprehensive review. *International  
213 Journal of Applied Earth Observation and Geoinformation*, 112:102926, 2022. ISSN 1569-8432.  
214 doi: <https://doi.org/10.1016/j.jag.2022.102926>. URL <https://www.sciencedirect.com/science/article/pii/S1569843222001248>.

216 [22] Qingyi Wang, Shenhao Wang, Yunhan Zheng, Hongzhou Lin, Xiaohu Zhang, Jinhua Zhao, and  
217 Joan Walker. Deep hybrid model with satellite imagery: How to combine demand modeling and  
218 computer vision for travel behavior analysis? *Transportation Research Part B: Methodological*,  
219 179:102869, 2024.

220 [23] Xuedong Lu and Eric I. Pas. Socio-demographics, activity participation and travel behavior.  
221 *Transportation Research Part A: Policy and Practice*, 33(1):1–18, 1999. ISSN 0965-8564. doi:  
222 [https://doi.org/10.1016/S0965-8564\(98\)00020-2](https://doi.org/10.1016/S0965-8564(98)00020-2). URL <https://www.sciencedirect.com/science/article/pii/S0965856498000202>.

223